Supporting Information

Flexible three-dimensional diacetylene functionalized covalent organic frameworks for ultrahigh iodine capture

Junyan Zou, [a] Dan Wen, [bc] and Yu Zhao*[bc]

[a] Guangdong Provincial Key Laboratory of Optical Fiber Sensing and Communications, Siyuan Laboratory, Guangzhou Key Laboratory of Vacuum Coating Technologies and New Energy Materials, Guangdong Provincial Engineering Technology Research Center of Vacuum Coating Technologies and New Energy Materials, Department of Physics, Jinan University, Guangzhou 510632, Guangdong, China.

[b] Zhejiang Engineering Laboratory for Green Syntheses and Applications of Fluorine-Containing Specialty Chemicals, Institute of Advanced Fluorine-Containing Materials, Zhejiang Normal University, Jinhua 321004, Zhejiang, China.

[c] Key Laboratory of the Ministry of Education for Advanced Catalysis Materials, Institute of Physical Chemistry, Zhejiang Normal University, Jinhua 321004, Zhejiang, China.

E-mail: zhaoyu@zjnu.edu.cn

Contents

Section S1. Materials and Characterizations

S1.1. Materials

All materials were reagent grade and used as received, unless stated otherwise.

4-iodobenzaldehyde (Aladdin®, ≥98.0%), 4-ethynylbenzaldehyde (Aladdin®, ≥98.0%), 1,3,5-trimethylbenzene (Aladdin®, ≥98.0%), triethylamine (TEA, Aladdin®, ≥99.0%) dichlorobis(triphenylphosphine)palladium(II) (J&K scientific LTD, 98.0%), copper(I) iodide (J&K scientific LTD, 98.0%), copper(II) acetate (J&K scientific LTD, ≥98.0%), iodine (J&K scientific LTD, ≥99.8%), 1,4-dioxane (Sinopharm chemical reagent Co., Ltd., ≥99.5%), tetrahydrofuran (THF, Sinopharm chemical reagent Co., Ltd., ≥99.0 %), methanol (Sinopharm chemical reagent Co., Ltd., ≥99.7%), dichloromethane (DCM, Sinopharm chemical reagent Co., Ltd., ≥99.5%), *n*-hexane (Sinopharm chemical reagent Co., Ltd., ≥97.0%), ethyl acetate (EA, Sinopharm chemical reagent Co., Ltd., ≥99.5%), acetone (Sinopharm chemical reagent Co., Ltd., ≥99.5%), *N*,*N*-Dimethylformamide (DMF, Sinopharm chemical reagent Co., Ltd., ≥99.5%), HCl 32% (Sinopharm chemical reagent Co., Ltd.), Na_2SO_4 (Sinopharm chemical reagent Co., Ltd., ≥99.0%), acetic acid (Sinopharm chemical reagent Co., Ltd., ≥99.5%), NaOH (Sinopharm chemical reagent Co., Ltd., ≥96.0%). The solvents were purified and dried according to the standard techniques: TEA, THF, methanol, 1,4-dioxane, 1,3,5-trimethylbenzene and pyridine was distilled from CaH_2.

S1.2. Characterizations

Nuclear magnetic resonance (NMR) spectroscopy. ^{1}H NMR spectra were measured on a Bruker Fourier 400 MHz spectrometer. Solid-state NMR spectra were recorded at ambient pressure on a Bruker Fourier 600 MHz spectrometer using a standard CP pulse sequence probe with 3.2 mm (outside diameter) zirconia rotors. Unless otherwise stated, all spectra were measured at ambient temperature. The chemical shift for ^{1}H-NMR spectra was reported in parts per million (ppm) and referenced to characteristic solvent signals of partly deuterated solvents: $CDCl_3$ at 7.26 ppm and DMSO-d_6 at 2.50 ppm. ^{13}C-NMR spectra were reported in ppm relative to characteristic signals of partly deuterated solvents: the centroid peak of the $CDCl_3$ triplet at 77.16 ppm and DMSO-d_6 at 39.52 ppm. The spin multiplicity and corresponding signal patterns were abbreviated as follows: s = singlet, d = doublet, t = triplet, q = quartet, quint. = quintet, sext. = sextet, m = multiplet and br = broad signal. Coupling constants *J* were noted in Hz.

Fourier transform infrared (FT-IR) spectroscopy. The FTIR spectra (KBr) were obtained using a SHIMADZU IRAffinity-1 Fourier transform infrared spectrophotometer. A SHIMADZU UV-2450 spectrophotometer was used for all absorbance measurements.

Powder X-ray diffraction (PXRD) analysis. Powder X-ray diffraction (PXRD) patterns were carried out in reflection mode on a Bruker D8 advance powder diffractometer with Cu Kα (λ = 1.5418 Å) line focused radiation at 40 kV and 40 mA from 2^{θ} = 1.0° up to 40° with 0.020481 increment by Bragg-Brentano. The powdered sample was added to the glass and compacted for measurement.

Thermogravimetric analysis (TGA). Thermogravimetric analysis (TGA) was recorded on a

SHIMADZU DTG-60 thermal analyzer under N_2. The operational range of the instrument was from 30 °C to 800 °C at a heating rate of 10 °C min^{-1} with N_2 flow rate of 30 mL min^{-1}.

Nitrogen isotherm measurements. Nitrogen sorption experiments were performed at 77 K up to 1 bar using a nanometric sorption analyzer The adsorption-desorption isotherms of N_2 were obtained at 77 K using a BELSORP MAX gas sorption analyzer. Before sorption analysis, the sample was evacuated at 100 ^oC for 12 h using a turbomolecular vacuum pump. Specific surface areas were calculated from nitrogen adsorption data by multipoint BET analysis. Nonlocal density functional theory (QS-DFT) was applied to analyze the N_2 isotherm based on the model of N_2@77 K on carbon with cylindrical pores.

Elemental analysis. The elemental analysis was performed on an Elementar Analysensysteme GmbH Vario EL cube elemental analyzer.

Scanning electron microscopy (SEM). Scanning electron microscopy (SEM) was performed on a Zeiss Gemini SEM 300 microscope instrument. Samples were prepared by dispersing the material onto conductive adhesive tapes attached to a flat aluminum sample holder and then coated with gold.

Energy dispersive spectroscopy (EDS). EDS analysis were performed on a Zeiss Gemini SEM 300 microscope instrument.

Transmission electron microscope (TEM). High resolution transmission electron microscope (HR-TEM) analysis was collected on a JEOL JEM-2100 microscope instrument at 200 kV. synthesized sample was dispersed into ethyl alcohol to obtain a highly dispersed suspension. Then, one droplet was transferred onto a carbon film supported TEM grid.

Section S2. Synthetic Procedures

Synthesis of 4,4'-(ethyne-1,2-diyl)dibenzaldehyde (EDDA).

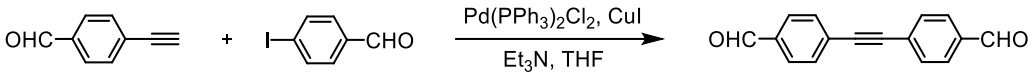

Under a nitrogen atmosphere, 4-iodobenzaldehyde (846 mg, 3.65 mmol, 1.00 eq.), 4-ethynylbenzaldehyde (475 mg, 3.65 mmol, 1.00 eq.), $Pd(PPh_3)_2Cl_2$ (128 mg, 183 µmol, 0.05 eq.) and CuI (35.0 mg, 183 µmol, 0.05 eq.) were dissolved in 50 mL of anhydrous THF. The mixture was purged for 5 minutes with an argon balloon and then was set under an argon funnel. Subsequently, Dry TEA (7.3 mL, 5.29 g, 52.3 mmol, 14.0 eq.) was added with a syringe, turning the solution to dark brown. After stirring for 16 h at room temperature, all volatiles were removed under reduced pressure. Purification via column chromatography using DCM/*n*-hexane [5:1] as eluent yielded the product as white crystals (556 mg, 2.37 mmol) in a yield of 65%. ^{1}H-NMR was in accordance with literature.[1]

^{1}H-NMR (400 MHz, $CDCl_3$): δ_H [ppm] = 10.04 (s, 2H), 7.90 (d, J = 7.6 Hz, 4H), 7.71 (d, J = 8.0 Hz, 4H);
^{13}C NMR (101 MHz, $CDCl_3$): δ_C [ppm] = 191.5, 136.0, 132.4, 129.7, 128.8, 92.2.

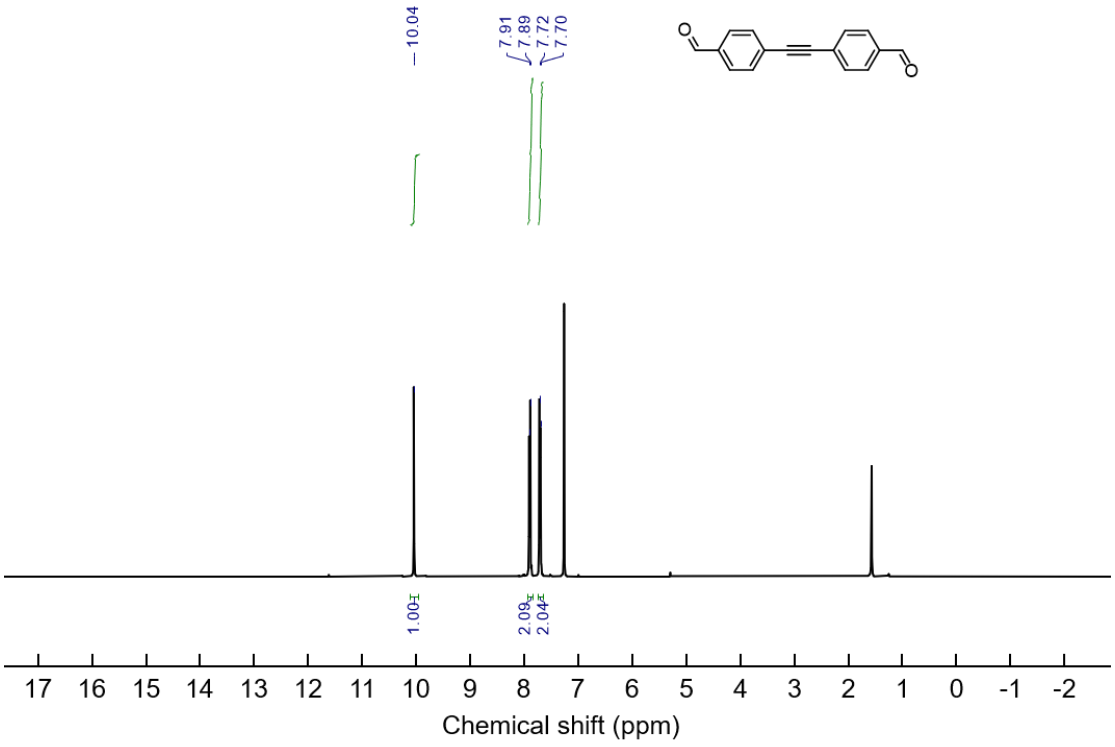

Fig. S1 The ^{1}H NMR spectra of 4,4'-(ethyne-1,2-diyl)dibenzaldehyde in $CDCl_3$.

Synthesis of 4,4'-(buta-1,3-diyne-1,4-diyl)dibenzaldehyde (BDDA).

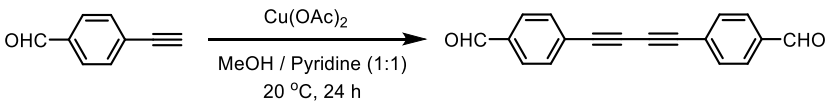

$Cu(OAc)_2$ (2.7 g, 15.0 mmol, 2.50 eq.) was added to a solution of 4-ethynylbenzaldehyde (781 mg, 6.0 mmol) in pyridine/MeOH 1:1 (v/v; 60 ml). After the solution was stirred at 20 °C for 24 h, all volatiles were removed under reduced pressure, purification via column chromatography using EA/*n*-hexane [1:4] as eluent yielded the product as pale-yellow powder (450 mg, 1.74 mmol) in a yield of 58%. ^{1}H-NMR was in accordance with literature.[2]

^{1}H-NMR (400 MHz, $CDCl_3$): δ_H [ppm] = 10.04 (s, 2H), 7.88 (d, J = 8.0 Hz, 4H), 7.69 (d, J = 8.0 Hz, 4H);

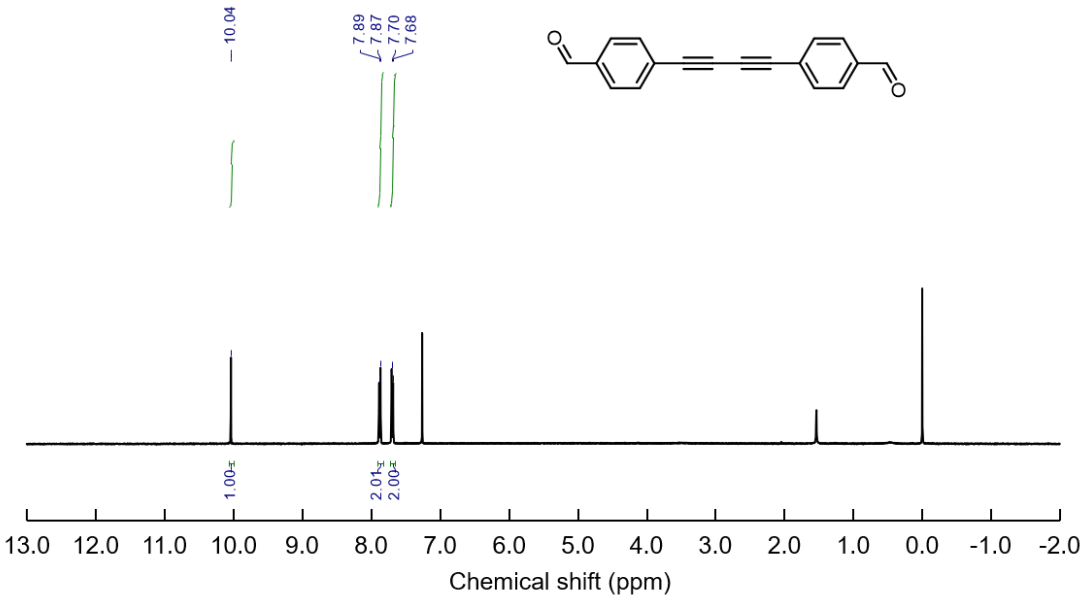

Fig. S2 The ^{1}H NMR spectra of 4,4'-(buta-1,3-diyne-1,4-diyl)dibenzaldehyde in $CDCl_3$.

Preparation of CPOF-2.

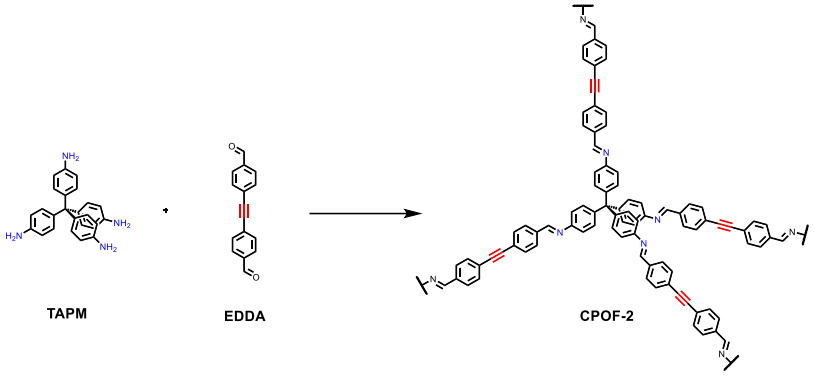

A Pyrex tube measuring o.d. × i.d. = 10 × 8 mm^2 was charged with tetra(4-aminophenyl)methane (TAPM, 19.0 mg, 0.05 mmol), 4,4'-(ethyne-1,2-diyl)dibenzaldehyde (EDDA, 23.4 mg, 0.10 mmol) in a mixed solution of 1,4-dioxane (0.4 mL), 1,3,5-trimethylbenzene (0.6 mL) and 6.0 M acetic acid (0.1 mL). The Pyrex tube was flash frozen in a liquid nitrogen bath sealed under vacuum. Upon warming to room temperature, the tube was placed in an oven at 120 °C for three days. The brown solid was isolated by filtration and washed with THF (3 × 15 mL), acetone (3 × 15 mL) and n-hexane (3 × 15 mL). The powder was dried at 80 ºC under vacuum overnight to afford the CPOF-2 as a brown crystalline solid (32.3 mg, Yield: 78%). Anal. Cald for $(C_{57}H_{36}N_4)_n$: C 88.15%; H 4.64%; N 7.21%. Found: C 86.46%; H 4.55%; N 7.11%.

Preparation of CPOF-3.

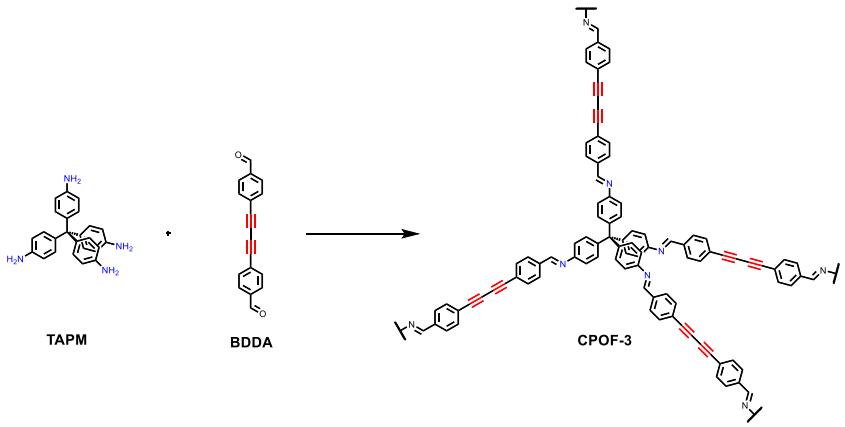

A Pyrex tube measuring o.d. × i.d. = 10 × 8 mm^2 was charged with tetra(4-aminophenyl)methane (TAPM, 19.0 mg, 0.05 mmol), 4,4'-(buta-1,3-diyne-1,4-diyl)dibenzaldehyde (BDDA, 25.8 mg, 0.10 mmol) in a mixed solution of 1,4-dioxane (0.4 mL), 1,3,5-trimethylbenzene (0.6 mL) and 6.0 M acetic acid (0.1 mL). The Pyrex tube was flash frozen in a liquid nitrogen bath sealed under vacuum. Upon warming to room temperature, the tube was placed in an oven at 120 °C for three days. The brown solid was isolated by filtration and washed with THF (3 × 15 mL), acetone (3 × 15 mL) and n-hexane (3 × 15 mL). The powder was dried at 80 ºC under vacuum overnight to afford the CPOF-3 as a brown crystalline solid (36.5 mg, Yield: 83%). Anal. Cald for $(C_{61}H_{36}N_4)_n$: C 88.85%; H 4.36%; N 6.79%. Found: C 87.34%; H 4.31%; N 6.38%.

Section S3. Fourier-transform infrared spectroscopy

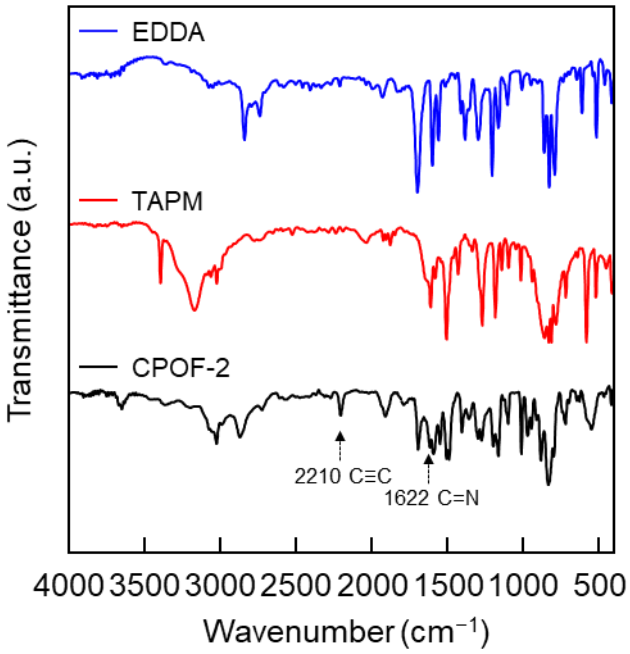

Fig. S3 FT-IR spectra of EDDA (blue), TAPM (red), CPOF-2 (black).

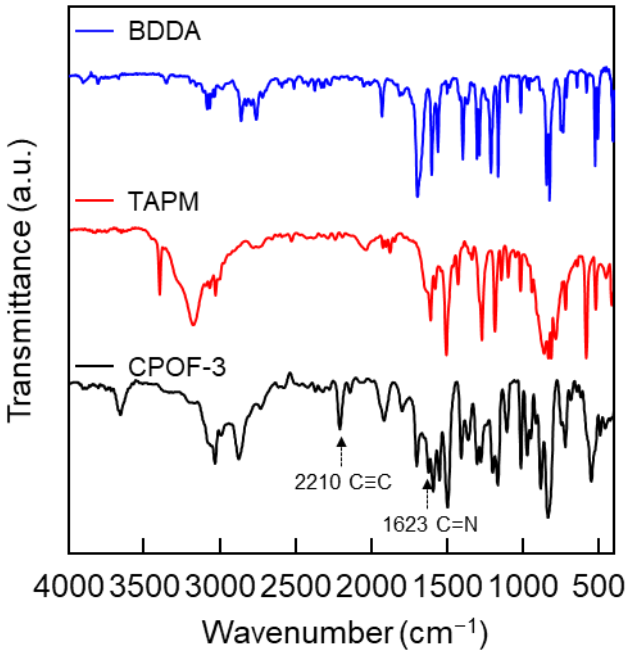

Fig. S4 FT-IR spectra of BDDA (blue), TAPM (red), CPOF-3 (black).

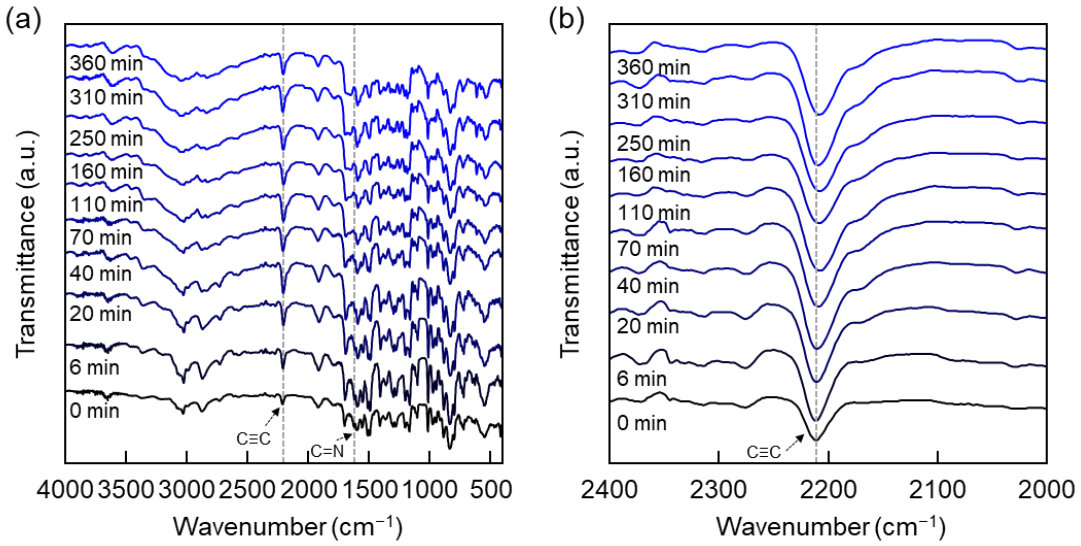

Fig. S5 Time-dependent FT-IR spectra of the I_2@CPOF-2 sample.

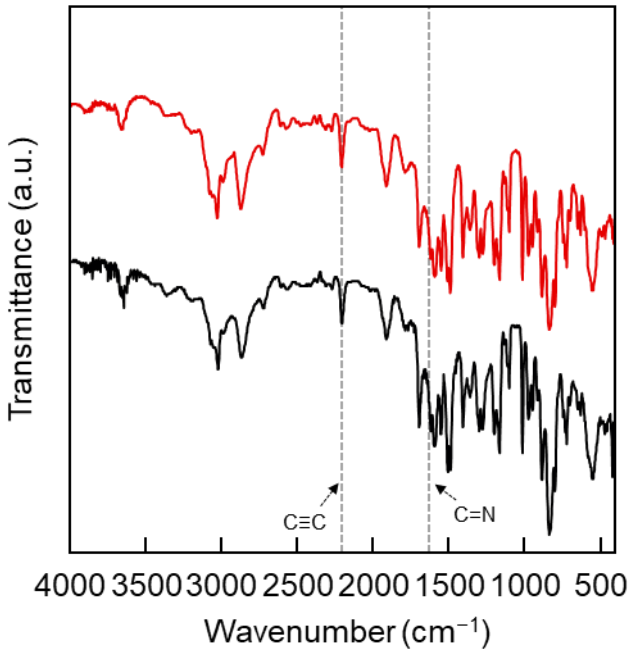

Fig. S6 Comparison of FT-IR spectra of the CPOF-2 upon five cycle use in vapor adsorption of iodine (black: pristine COFs; red: after five cycles).

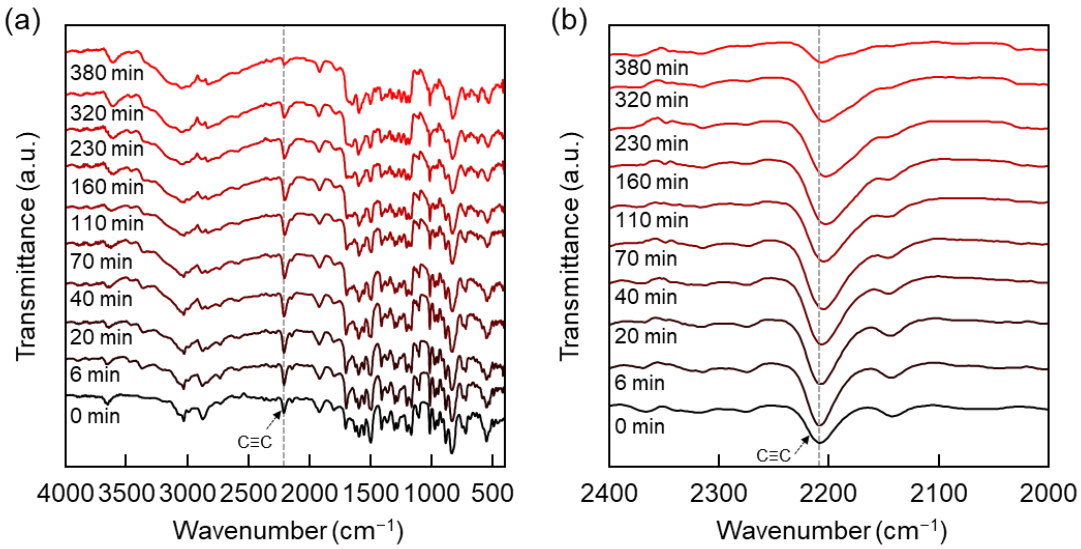

Fig. S7 Time-dependent FT-IR spectra of the I_2@CPOF-3 sample.

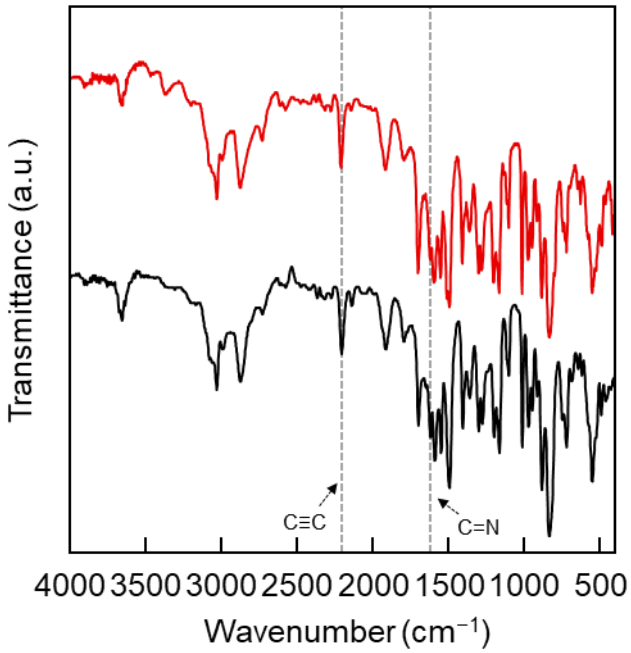

Fig. S8 Comparison of FT-IR spectra of the CPOF-3 upon five cycle use in vapor adsorption of iodine (black: pristine COFs; red: after five cycles).

Section S4. EDS analysis

Fig. S9 EDS elemental content analysis from SEM-related EDS in CPOF-2.

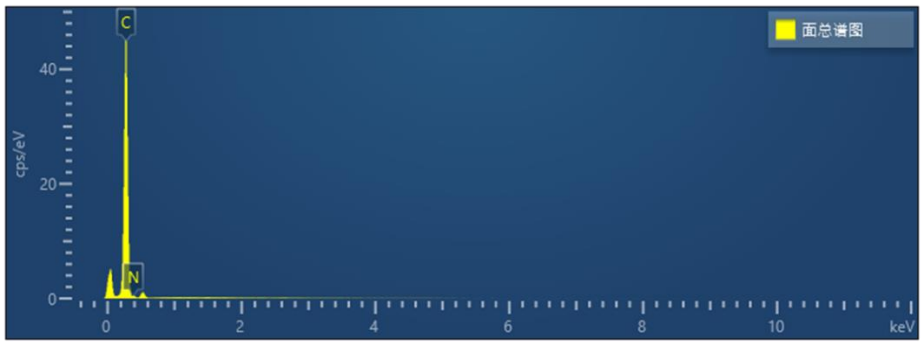

Fig. S10 EDS elemental content analysis from SEM-related EDS in CPOF-3.

Section S5. Solid-state ^{13}C NMR spectra

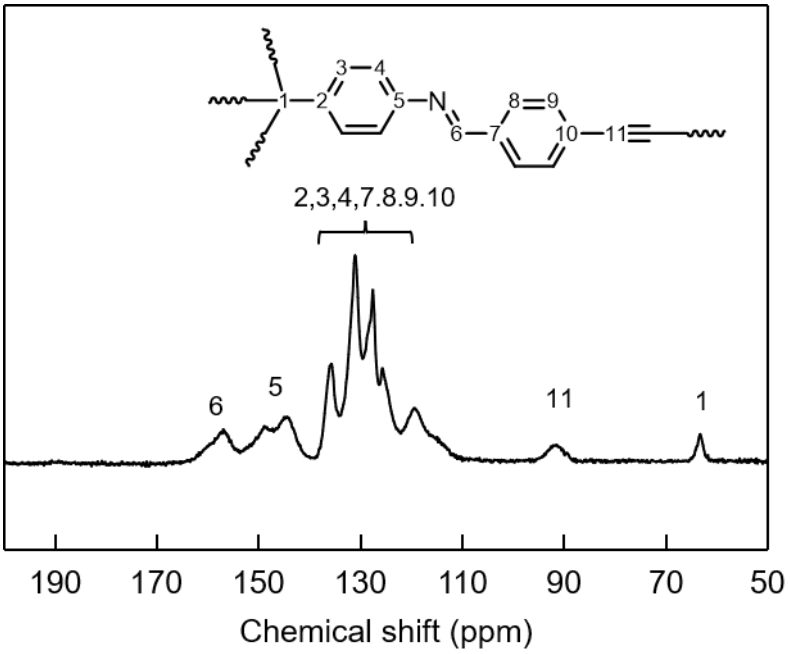

Fig. S11 Solid-state ^{13}C NMR of CPOF-2.

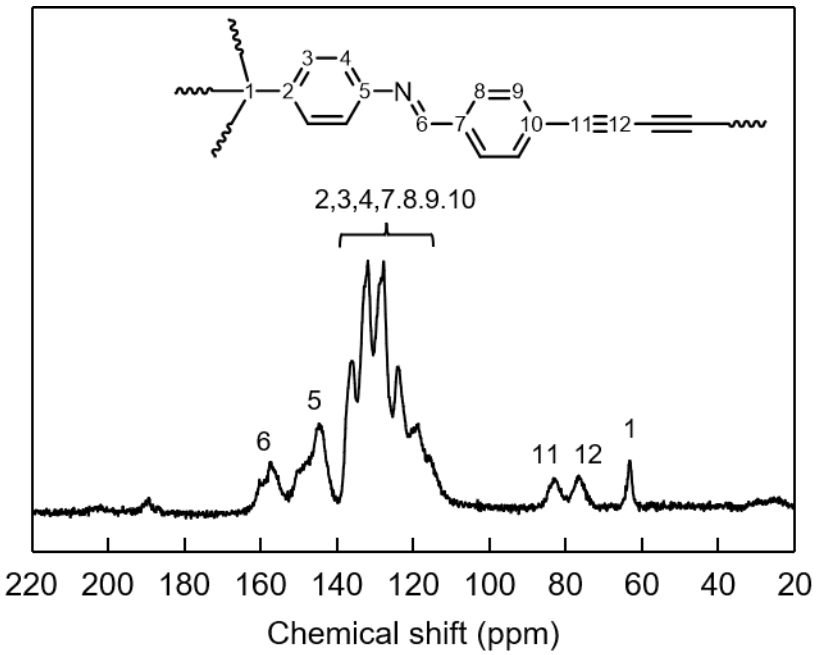

Fig. S12 Solid-state ^{13}C NMR of CPOF-3.

Section S6. TGA curves

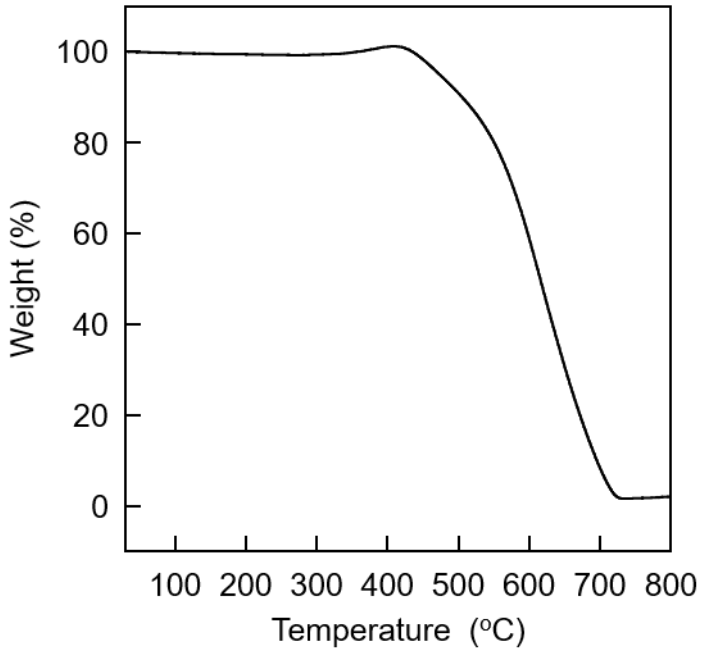

Fig. S13 TGA curve of CPOF-2 at the heating rate of 10 °C min^{-1} to 800 °C under the N_2 atmosphere with an N_2 flow rate of 20 mL min^{-1}.

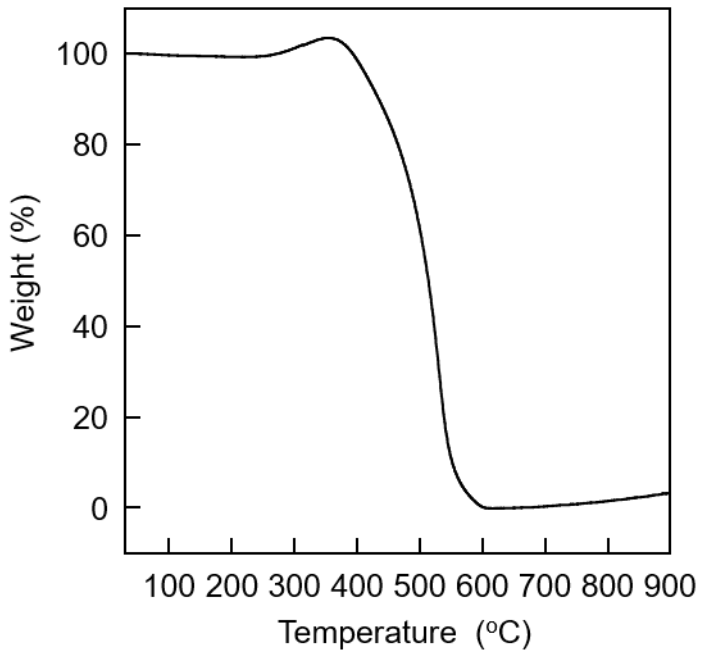

Fig. S14 TGA curve of CPOF-3 at the heating rate of 10 °C min^{-1} to 900 °C under the N_2 atmosphere with an N_2 flow rate of 20 mL min^{-1}.

Section S7. SEM image

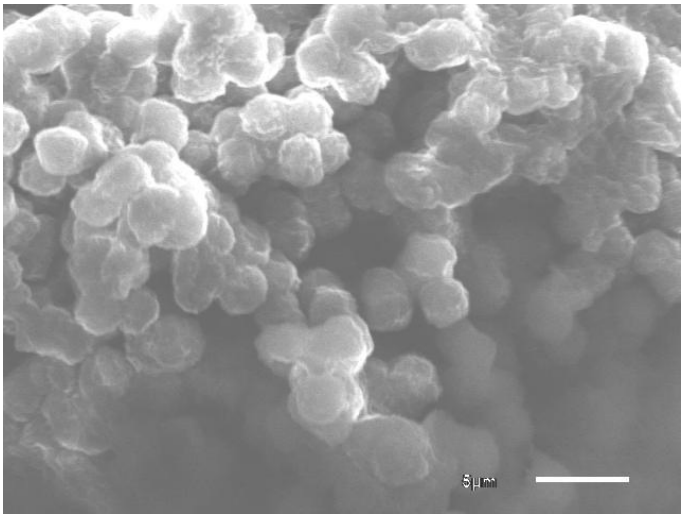

Fig. S15 SEM image of as-synthesized CPOF-2.

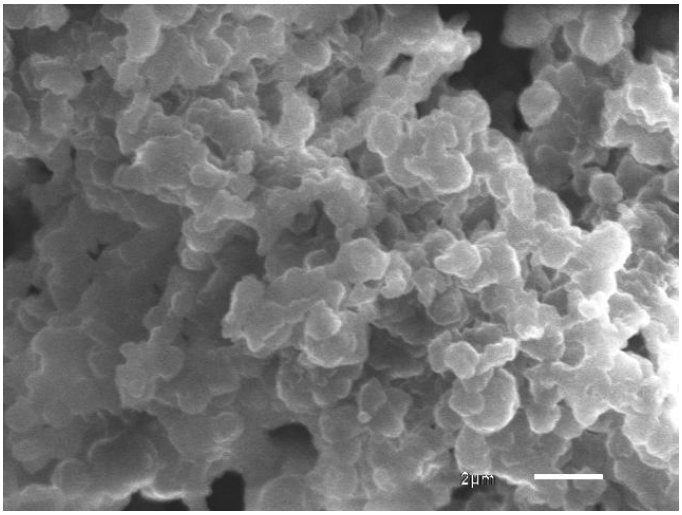

Fig. S16 SEM image of as-synthesized CPOF-3.

Section S8. TEM image

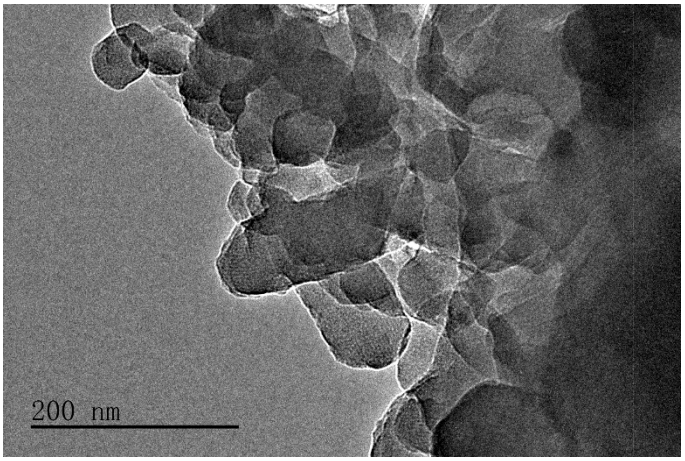

Fig. S17 TEM image of as-synthesized CPOF-2.

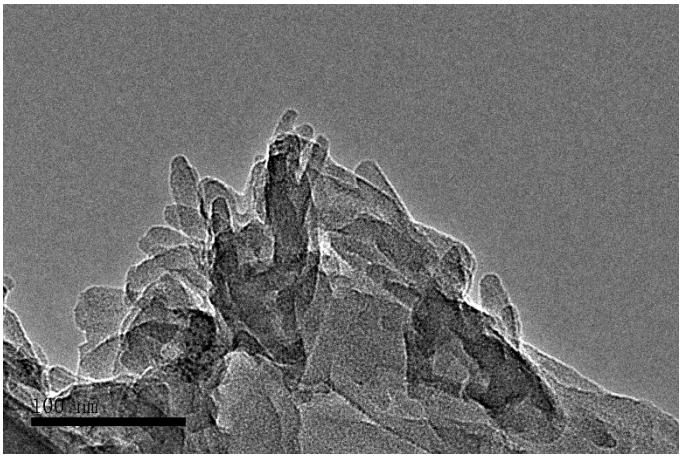

Fig. S18 TEM image of as-synthesized CPOF-3.

Section S9. PXRD patterns and structures

Crystal models for 3D-COFs were established by Materials Studio 7.0 Software Package. Geometry optimization of the established models was performed by Materials Studio Forcite Module, which is an advanced classical molecular mechanics tool and allows for fast and reliable geometry optimization and energy calculations. Optimized cell parameters were obtained at the same time. Possible structures with different degrees of interpenetration were tested in comparison with the experimental Powder X-ray diffraction (PXRD) data. Pawley refinement was carried out using Reflex, a software package for crystal determination from PXRD pattern. The Pawley refinement was performed to optimize the lattice parameters iteratively until the R*wp* and R*p* value converges and the overlay of the observed with refined profiles shows good agreement.

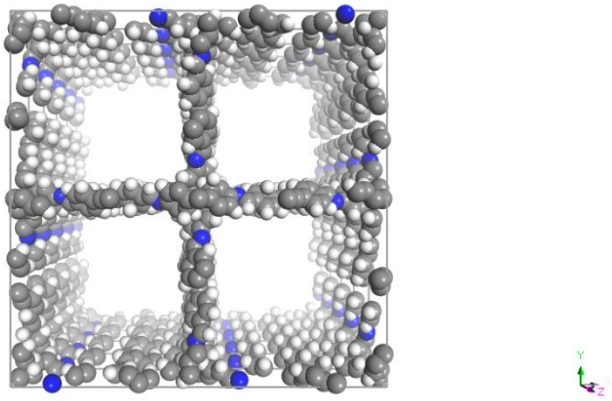

Fig. S19 Space-filling models of CPOF-2 with nine-interpenetrated **dia** net. Carbon, gray; Nitrogen, blue; Hydrogen, white.

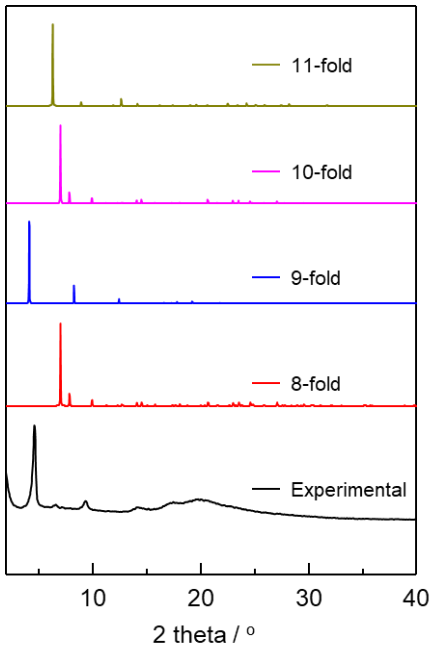

Fig. S20 Simulated PXRD patterns for possible isomers of CPOF-2 with different interpenetration degrees from 8 to 11 (8-fold, red; 9-fold, blue; 10-fold, purple; 11-fold, dark yellow) It can be seen that only the simulated PXRD pattern with 9-fold interpenetrated structure matches with the experimental data well.

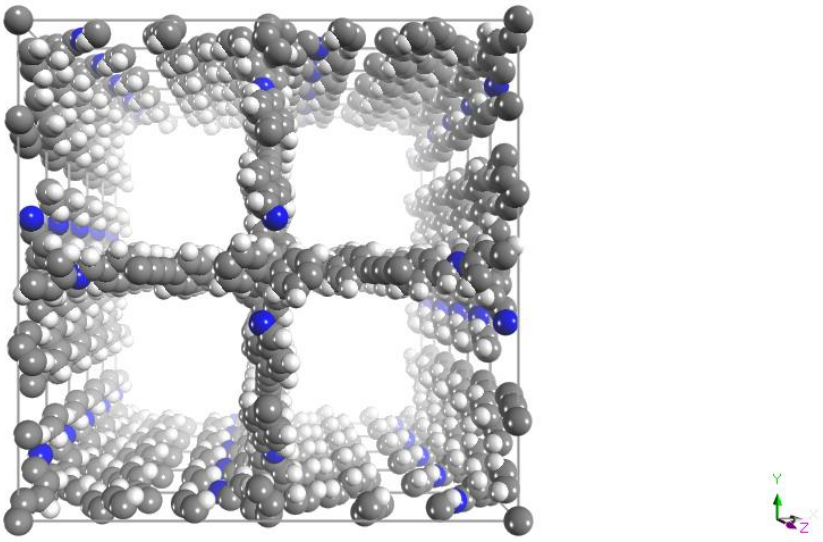

Fig. S21 Space-filling models of CPOF-3 with eleven-interpenetrated **dia** net. Carbon, gray; Nitrogen, blue; Hydrogen, white.

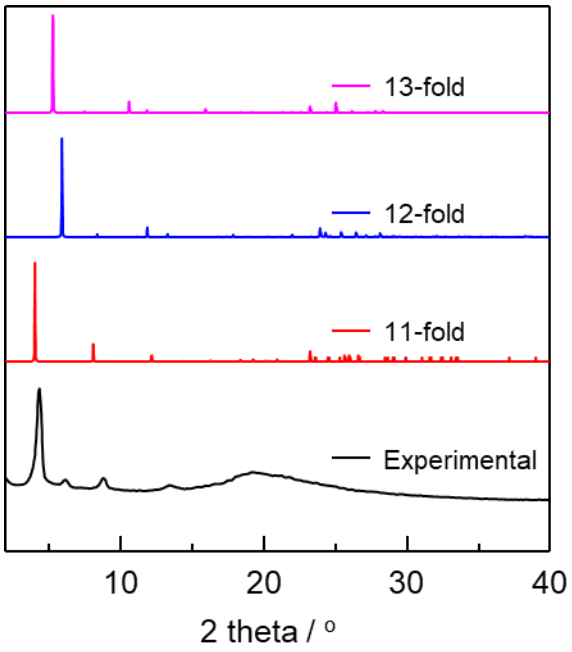

Fig. S22 Simulated PXRD patterns for possible isomers of CPOF-3 with different interpenetration degrees from 11 to 13 (11-fold, red; 12-fold, blue; 13-fold, purple) It can be seen that only the simulated PXRD pattern with 11-fold interpenetrated structure matches with the experimental data well.

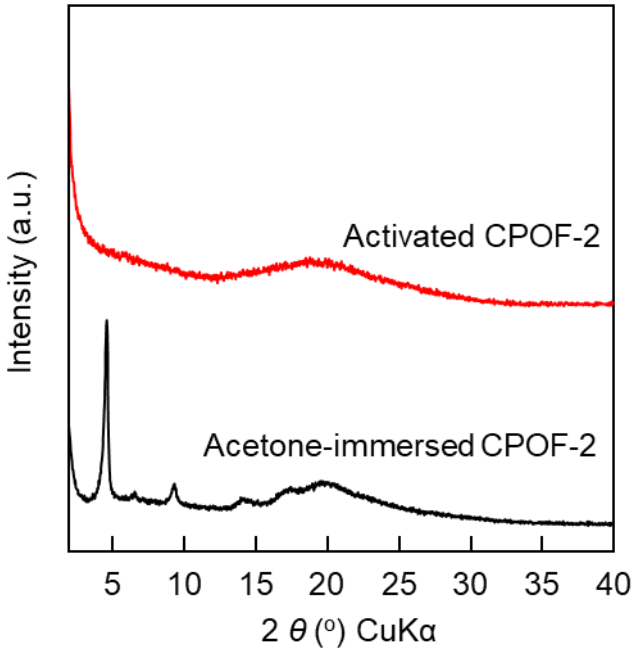

Fig. S23 PXRD pattern of CPOF-2 immersed with acetone (black) and activated CPOF-2 (red).

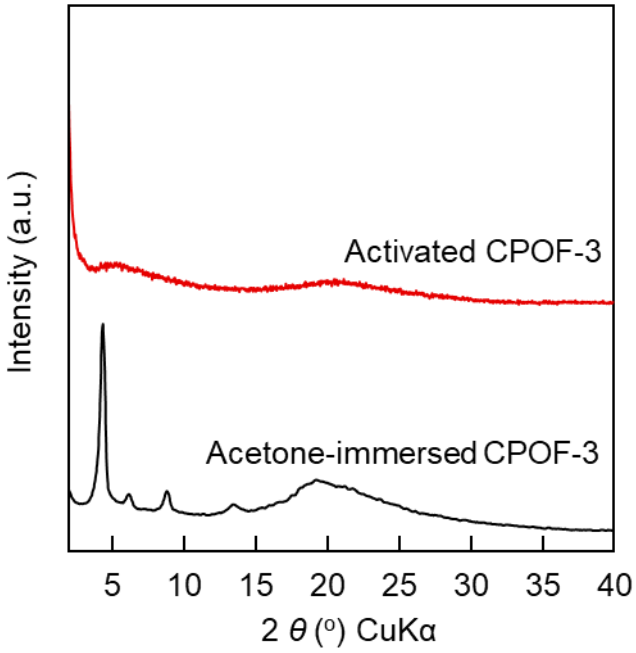

Fig. S24 PXRD pattern of CPOF-3 immersed with acetone (black) and activated CPOF-2 (red).

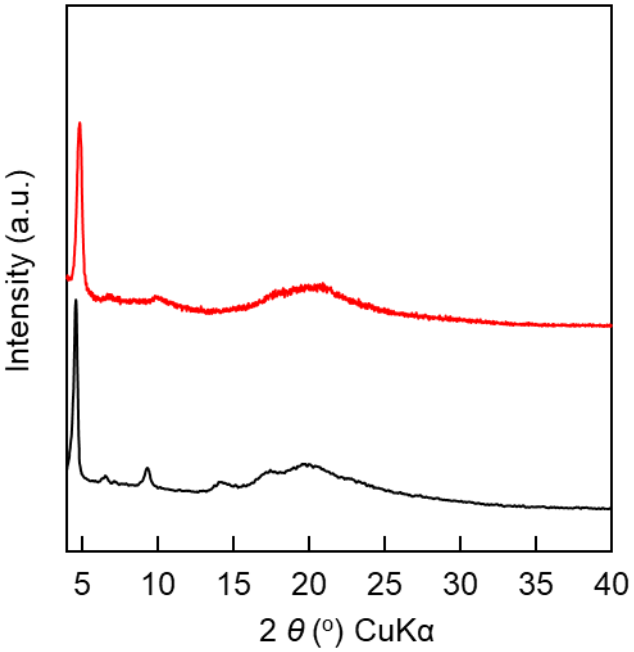

Fig. S25 Comparison of PXRD patterns of the CPOF-2 upon five cycle use in vapor adsorption of iodine (black: pristine COFs; red: after five cycles)

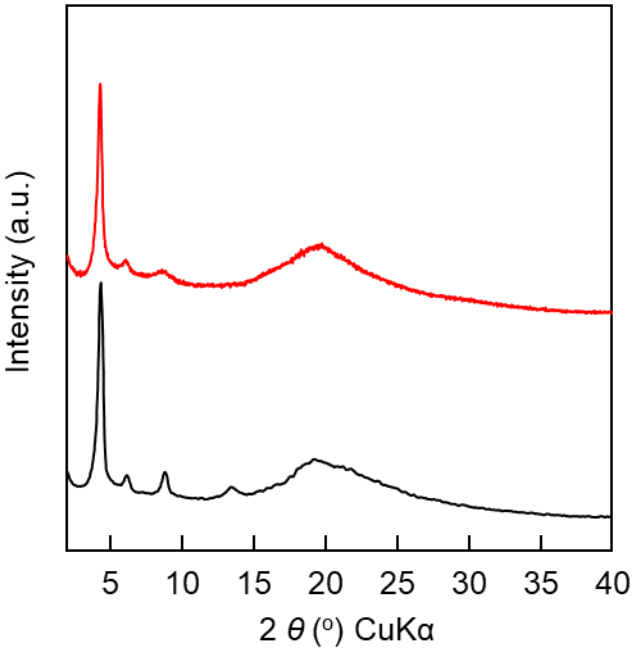

Fig. S26 Comparison of PXRD patterns of the CPOF-3 upon five cycle use in vapor adsorption of iodine (black: pristine COFs; red: after five cycles)

Section S10. Nitrogen adsorption

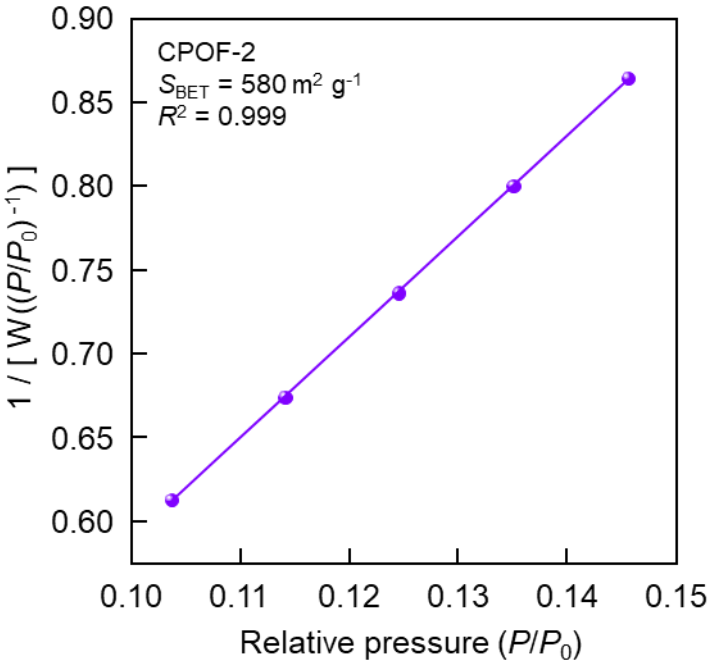

Fig. S27 BET plots of CPOF-2 calculated from N_2 adsorption isotherm at 77 K.

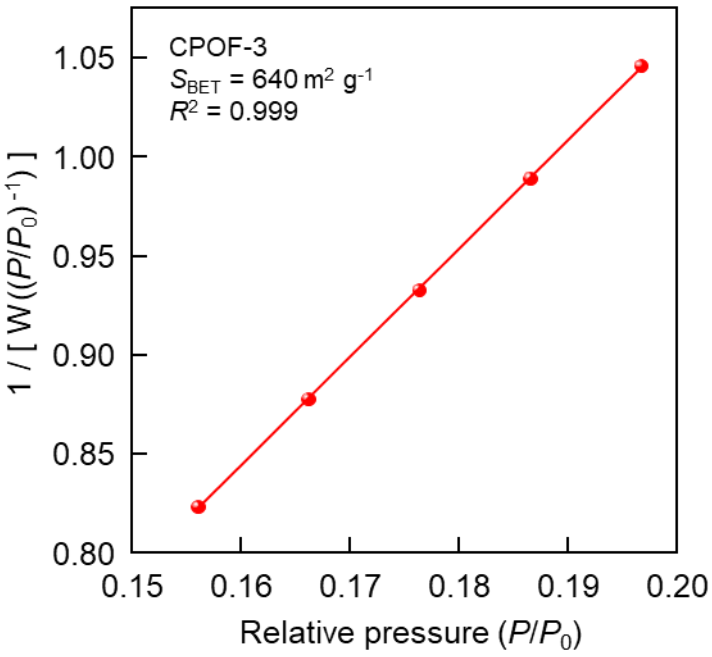

Fig. S28 BET plots of CPOF-3 calculated from N_2 adsorption isotherm at 77 K.

Section S11. Chemical stability tests

Both samples were dispersed in various solutions, such as tetrahydrofuran (THF), *N,N*-Dimethylformamide (DMF), aqueous HCl (0.1 M) and NaOH (0.1 M) solutions at room temperature for 24 hours. After that, the samples were thoroughly washed with acetone and then soaked in acetone for PXRD characterization. The results showed that the samples treated with different solvents still exhibited intense PXRD patterns without obvious change in the peak position and intensity, indicating that these COFs still maintained high crystallinity under harsh conditions. Meanwhile, the peak intensity of COFs is weakened due to the hydrolysis of the imine bonds under acidic conditions, which is a problem faced by most Schiff base COFs.

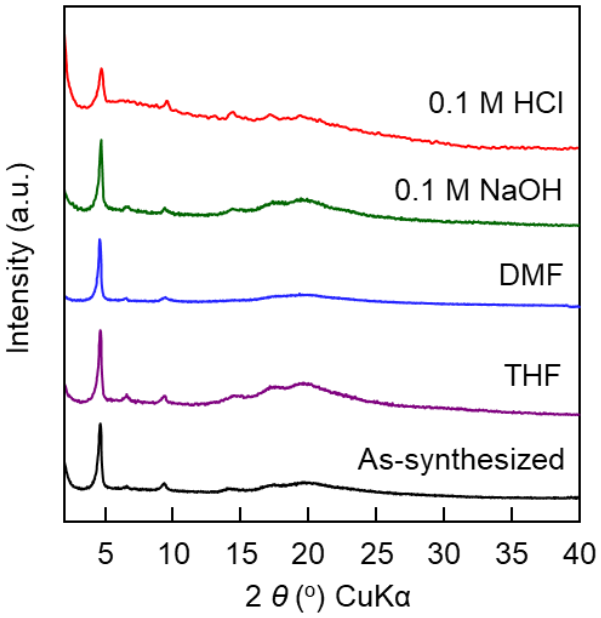

Fig. S29 PXRD patterns of CPOF-2 after the treatment in different organic solvents for 24 h.

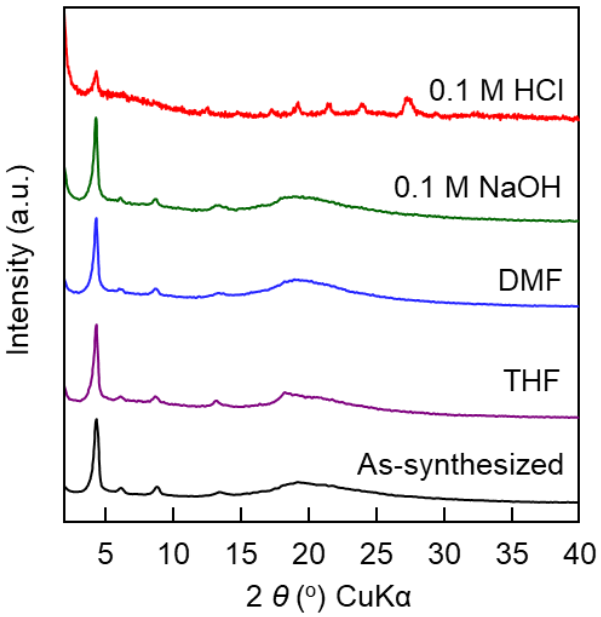

Fig. S30 PXRD patterns of CPOF-3 after the treatment in different organic solvents for 24 h.

Section S12. Iodine uptake experiments

Vapor-phase iodine uptake measurements were performed by simulating the typical nuclear waste processing.[3] In a typical experiment, about 30 mg of the sample was weighed into a brown vial, and then the vial was loaded into a larger brown vessel containing iodine powder. Afterward, the vessel was sealed and heated at 75 °C in a convection oven. At particular time intervals, the brown vial was removed, cooled to room temperature, and weighed. The uptake capacity was calculated by subtracting the initial mass and dividing the result by the initial mass: $(m_t - m_0)/m_0$. The samples were recycled by washing with ethanol and reused for further iodine uptake experiments.

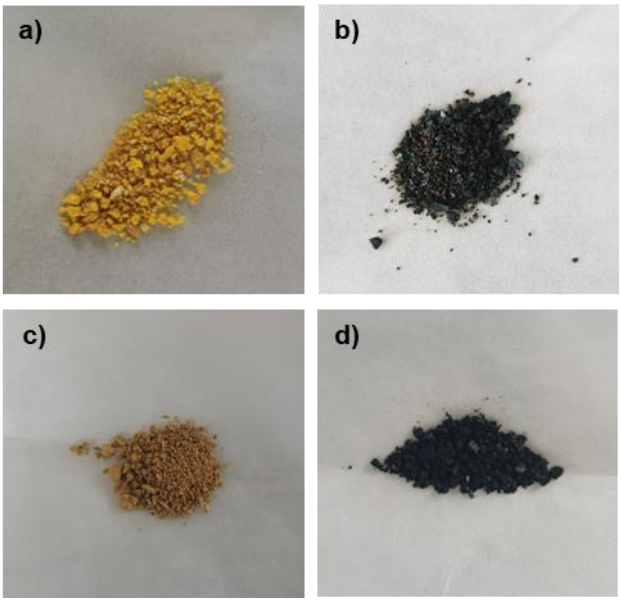

Fig. S31 The images of the COFs samples before (a: CPOF-2, c: CPOF-3) and after (b: I_2@CPOF-2, d: I_2@CPOF-3) the vapor phase iodine uptake.

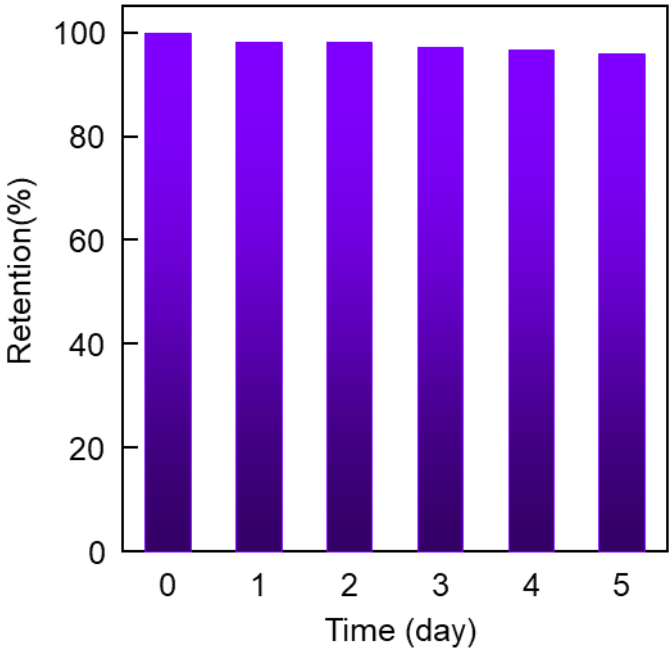

Fig. S32 Iodine retention of the iodine-captured CPOF-2 upon exposure to air at 298 K and ambient pressure.

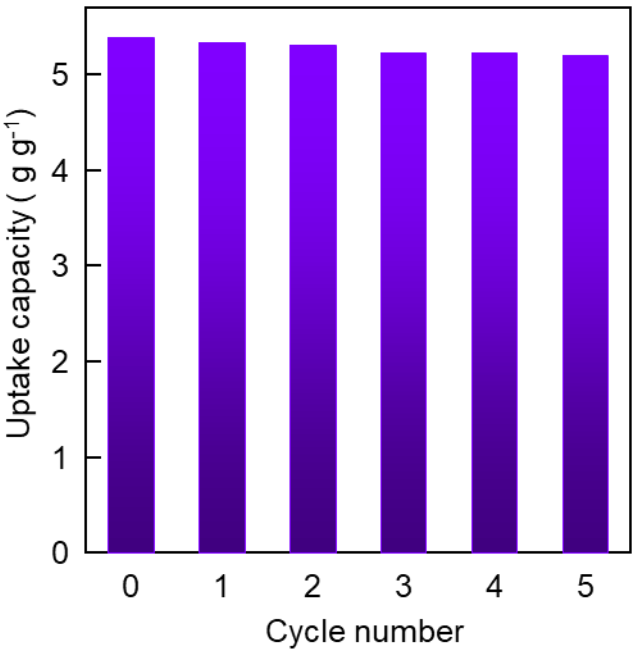

Fig. S33 Recycle performance towards iodine uptake of CPOF-2.

Table S1. The comparison of iodine uptake performances of CPOF-2 and CPOF-3 samples with previously reported adsorbents.

Adsorbent	S_{BET} (m^2 g^{-1})	Temperature (K)	Uptake (g g^{-1})	References
iCOF-AB-50	1390	348	10.21	[4]
COF-TAPT	2348	348	8.61	[5]
JUC-561	2358	348	8.19	[6]
COF-TAPB	2290	348	7.94	[5]
TFB-DB COF	734	348	6.40	[7]
QTD-COF-V	-	348	6.29	[8]
TPB-DMTP	1927	348	6.26	[9]
SCU-COF-2	413	348	6.00	[10]
CPOF-3	**640**	**348**	**5.87**	**This work**
Tfp-DB	158	348	5.82	[11]
TJNU-201	2510	350	5.63	[12]
TFPB-PyTTA-COF	1897	350	5.62	[13]
TPT-BD	109	348	5.43	[14]
Tfp-BD	138	348	5.42	[11]
CPOF-2	**580**	**348**	**5.40**	**This work**
COF-LZU1	858	350	5.30	[15]
TAPA-PDA COF	685	350	5.09	[16]
TFB-TD COF	221	348	4.97	[7]
TTA-TTB	1733	348	4.95	[9]
CSU-CPOPs-1	1032	348	4.94	[17]
TTPPA	512	350	4.90	[18]
SIOC-COF-7	618	348	4.81	[19]
ETTA-TPA	1822	348	4.79	[9]
PCMP-Y5	1212	358	4.75	[20]
COF-DL229	1749	348	4.70	[21]
QTD-COF-V	-	348	4.67	[22]
H-C-CTPs	640	348	4.60	[23]
COF-PA	1471	350	4.47	[24]
TTPB	222	350	4.43	[25]
CMP-LS5	1185	343	4.40	[26]
COF-320	2400	348	4.00	[27]
Meso-COF-3	982	348	4.00	[27]
FcTz-POP	410	348	3.96	[28]
OMC3	80	350	3.78	[29]
POP-2	41	353	3.76	[30]
KOH-AC	1973	350	3.76	[31]
COF-300	1360	348	3.50	[27]
HCMP-3	50	358	3.36	[32]
P-TzTz	137	350	3.26	[33]

TALPOP	401	353	3.14	[34]
Azo-PPN	400	350	2.90	[35]
BTT-TAPT-COF	864	348	2.76	[36]
PAF-24	321	348	2.76	[37]
PAF-23	273	348	2.71	[37]
COF-TpgDB	1163	348	2.60	[38]
PAF-25	403	348	2.60	[37]
Cg-5C	360	298	2.39	[39]
Azo-Trip	501	350	2.38	[40]
Uassis-PC800	3053	350	2.25	[41]
MALP-1	1179	350	2.09	[42]
CMPN-3	1368	343	2.08	[43]
NiP-CMP	2630	350	2.02	[44]
PAF-1	5600	333	1.86	[45]
HKUST-1	1850	348	1.75	[46]
MFM-300 (Sc)	1250	353	1.54	[47]
Pha-H_cOP-1	217	353	1.31	[48]
ZIF-8	1630	348	1.25	[49]
MFM-300 (In)	1050	353	1.16	[47]
Ag-MOR	-	368	0.28	[50]

Section S13. Kinetic studies of iodine adsorption

The pseudo-first-order and pseudo-second-order kinetic models were used to study the adsorption kinetics of iodine solution according to equation (1) and equation (2), respectively.

$$Q_t = Q_e(1 - exp\ (-k_1 t)) \qquad \text{equation (1)}$$

$$Q_t = (k_2 Q_e^2 t)/(1 + k_2 Q_e t) \qquad \text{equation (2)}$$

where Q_e (g g^{-1}) and Q_t (g g^{-1}) are the adsorption capacity at equilibrium and time t (h), respectively. k_1 (h^{-1}) and k_2 (h^{-1}) are the rate constant of pseudo-first-order and pseudo-second-order adsorption, respectively.

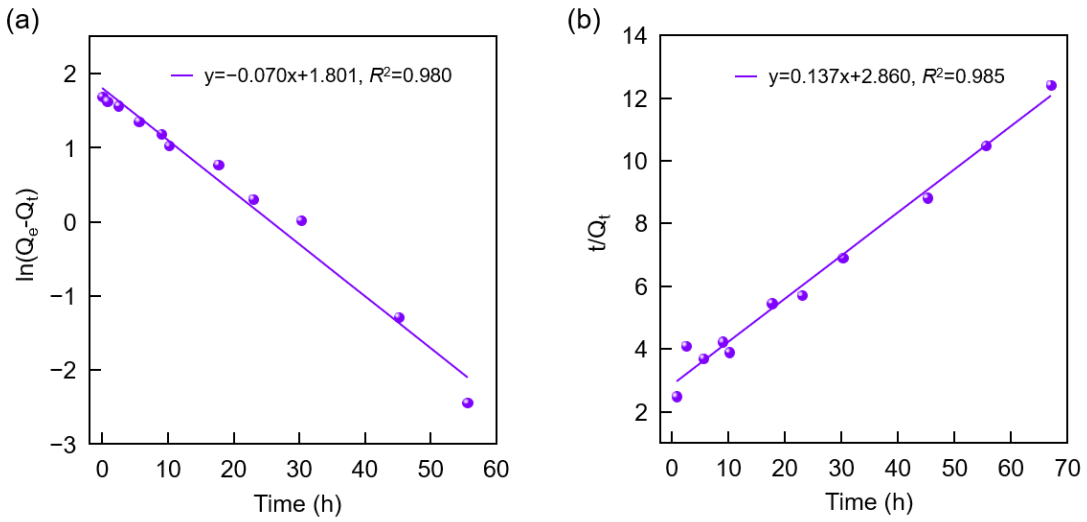

Fig. S34 The fitting curves for (a) pseudo-first-order and (b) pseudo-second-order kinetic model for the volatile iodine adsorption onto CPOF-2.

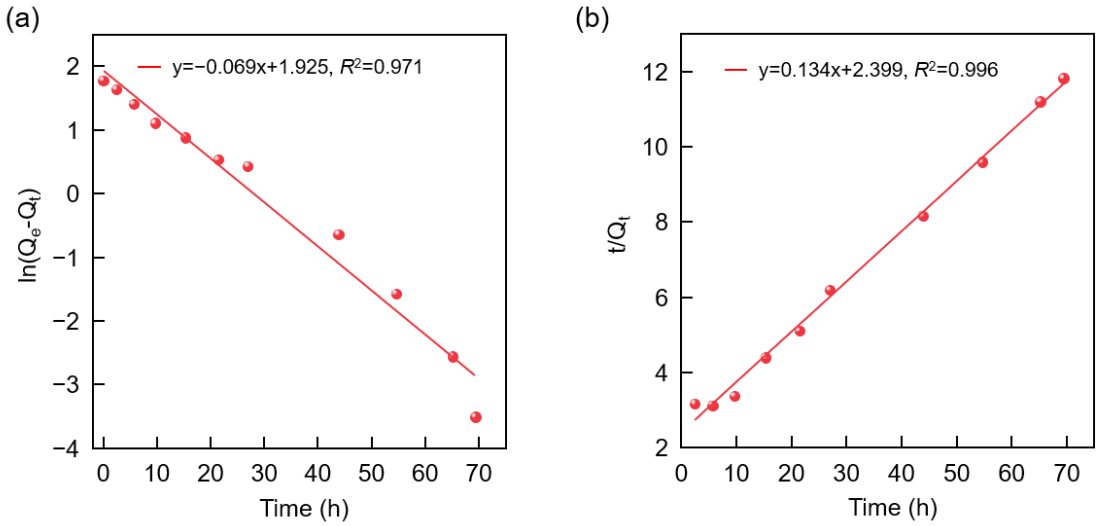

Fig. S35 The fitting curves for (a) Pseudo-first-order and (b) pseudo-second-order kinetic model for the volatile iodine adsorption onto CPOF-3.

Section S14. Electrical conductivity measurements

Electrochemistry experiments were conducted on a CHI660C Electrochemical Workstation (Shanghai ChenHua Electrochemical Instrument). Two pieces of gold with wires are attached to both sides of the sample. AC impedance was measured from 100 to 10^6 Hz with initial voltage of 0.0 V, and amplitude of 200 mV and quiet time of 1 s. COFs and I_2@COFs was pressed into a pellet, diameter = 0.5 cm, thickness = 0.5 cm. The conductivity of the pellet was determined by the following formula:

$$\sigma = \frac{w}{AR_e}$$

where w is the width of the pellet in cm, A the area in cm^2 and R_e the resistance at the electrolyte, which corresponds to the real component (Z') of the impedance at high frequencies.

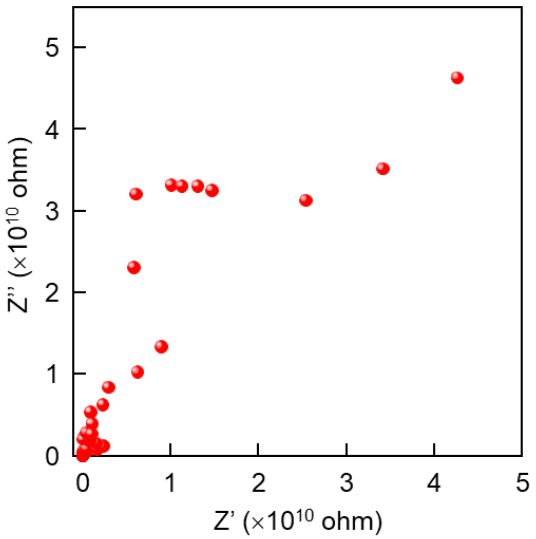

Fig. S36 Nyquist plot (frequency ranges from 10^6 to 1 Hz) of CPOF-3.

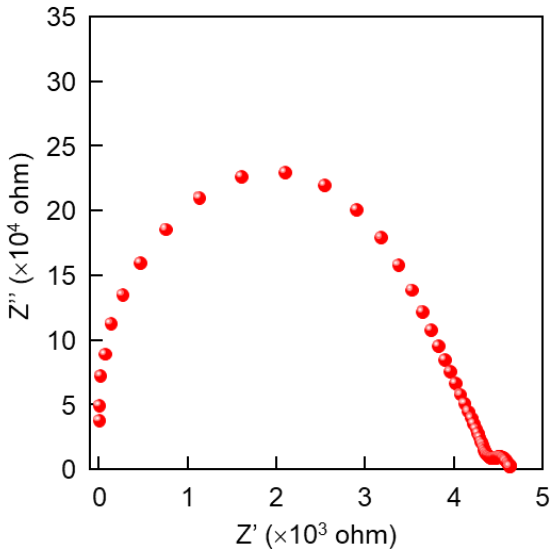

Fig. S37 Nyquist plot (frequency ranges from 10^6 to 1 Hz) of I_2@CPOF-3.

Table S2. Unit cell parameters and fractional atomic coordinates for CPOF-2 calculated based on the 9-fold interpenetrated **dia** net.

Space group		*I4₁/a* (No. 88)	
Unit cell		$a = b = 40.5302$ Å, $c = 7.1003$ Å, $\alpha = \beta = \gamma = 90^{o}$	
Pawley refinement		$R_p = 2.07\%$, $R_{wp} = 3.44\%$	
Atoms	x	y	z
C	0.52540	0.46594	0.26628
C	0.52624	0.43897	0.38864
C	0.50149	0.41514	0.38396
C	0.47499	0.41911	0.25899
C	0.4738	0.44624	0.13769
C	0.49973	0.46961	0.13316
C	0.48833	0.36013	0.49798
N	0.50300	0.38847	0.51639
C	0.50672	0.34158	0.81863
C	0.50909	0.31719	0.95733
C	0.49573	0.28586	0.92519
C	0.47970	0.27905	0.75503
C	0.47742	0.30336	0.61588
C	0.49099	0.33479	0.64629
C	0.49872	0.26060	1.06608
H	0.54513	0.48396	0.27299
H	0.54634	0.43631	0.48743
H	0.45448	0.40207	0.25986
H	0.45198	0.44887	0.05183
H	0.47461	0.35427	0.37140
H	0.51714	0.36575	0.84536
H	0.52139	0.32268	1.08924
H	0.46921	0.25485	0.72968
H	0.46520	0.29759	0.48418
C	0.50000	0.50000	0.00000

Table S3. Unit cell parameters and fractional atomic coordinates for CPOF-3 calculated based on the 11-fold interpenetrated **dia** net.

Space group		*I4₁/a* (No. 88)	
Unit cell		$a = b = 43.6198$ Å, $c = 6.5346$ Å, $\alpha = \beta = \gamma = 90^{o}$	
Pawley refinement		$R_p = 1.61\%$, $R_{wp} = 2.84\%$	
Atoms	x	y	z
C	0.47458	0.04916	0.90289
C	0.47628	0.07558	1.02300
C	0.50209	0.08108	1.14500
C	0.52584	0.05981	1.14664
C	0.52430	0.03337	1.02691
C	0.49937	0.02826	0.89380
C	0.48784	0.13130	1.27601
N	0.50360	0.10611	1.28604
C	0.47592	0.18281	1.41825
C	0.47798	0.20467	1.57404
C	0.49435	0.19804	1.75274
C	0.50860	0.16956	1.77644
C	0.50664	0.14773	1.62086
C	0.49036	0.15425	1.44011
C	0.49874	0.23911	2.04638
C	0.49664	0.22044	1.91209
H	0.45336	0.04514	0.82233
H	0.45671	0.09075	1.02771
H	0.54559	0.06405	1.24194
H	0.54323	0.01733	1.03057
H	0.47293	0.13597	1.14721
H	0.46319	0.18819	1.28053
H	0.46689	0.22673	1.55546
H	0.52121	0.16430	1.91503
H	0.51766	0.12569	1.64165
C	0.50000	0.00000	0.75000

Section S15. References

1 R. L. Greenaway, V. Santolini, M. J. Bennison, B. M. Alston, C. J. Pugh, M. A. Little, M. Miklitz, E. G. B. Eden-Rump, R. Clowes, A. Shakil, H. J. Cuthbertson, H. Armstrong, M. E. Briggs, K. E. Jelfs and A. I. Cooper, *Nat. Commun.*, 2018, **9**, 2849.

2 M. Wierzbicka, I. Bylinska, A. Sikorski, C. Czaplewski and W. Wiczk, *Photochem. Photobiol. Sci.*, 2015, **14**, 2251−2260.

3 S. Walker, R. A. Hyde, R. B. Piper and Roy, M. W. An overview of in situ waste treatment technologies. Spectrum 92: nuclear and hazardous waste management international topical meeting, Boise, ID, Aug 23−27, 1992; American Nuclear Society, 1992; p 12.

4 Y. Xie, T. Pan, Q. Lei, C. Chen, X. Dong, Y. Yuan, J. Shen, Y. Cai, C. Zhou, I. Pinnau and Y. Han, *Angew. Chem., Int. Ed.*, 2021, **60**, 22432−22440.

5 Y. Xie, T. Pan, Q. Lei, C. Chen, X. Dong, Y. Yuan, W. A. Maksoud, L. Zhao, L. Cavallo, I. Pinnau and Y. Han, *Nat. Commun.*, 2022, **13**, 2878.

6 J. Chang, H. Li, J. Zhao, X. Guan, C. Li, G. Yu, V. Valtchev, Y. Yan, S. Qiu and Q. Fang, *Chem. Sci.*, 2021, **12**, 8452−8457.

7 S. Song, Y. Shi, N. Liu and F. Liu, *ACS Appl. Mater. Interfaces*, 2021, **13**, 10513−10523.

8 X. Guo, Y. Li, M. Zhang, K. Cao, Y. Tian, Y. Qi, S. Li, K. Li, X. Yu and L. Ma, *Angew. Chem., Int. Ed.*, 2020, **59**, 22697−22705.

9 P. Wang, Q. Xu, Z. Li, W. Jiang, Q. Jiang and D. Jiang, *Adv. Mater.*, 2018, **30**, 1801991−1801997.

10 L. W. He, L. Chen, X. L. Dong, S. T. Zhang, M. X. Zhang, X. Dai, X. J. Liu, P. Lin, K. F. Li, C. L. Chen, T. T. Pan, F. Y. Ma, J. C. Chen, M. J. Yuan, Y. G. Zhang, L. Chen, R. H. Zhou, Y. Han, Z. F. Chai and S. A. Wang, *Chem*, 2021, **7**, 699−714.

11 S. Song, Y. Shi, N. Liu and F. Liu, *RSC Adv.*, 2021, **11**, 10512−10523.

12 J. Li, H. Zhang, L. Zhang, K. Wang, Z. Wang, G. Liu, Y. Zhao and Y. Zeng, *J. Mater. Chem. A*, 2020, **8**, 9523−9527.

13 M. Zhou, Z. Li, A. Munyentwali, C. Li, H. Shui and H. Li, *Chem. Asian J*, 2022, **17**, e202200358.

14 X. Guo, Y. Tian, M. Zhang, Y. Li, R. Wen, X. Li, X. Li, Y. Xue, L. Ma, C. Xia and S. Li, *Chem. Mater.*, 2018, 30, 2299−2308.

15 Y. Yang, X. Xiong, Y. Fan, Z. Lai, Z. Xu and F. Luo, *J. Solid State Chem.*, 2019, **279**, 120979.

16 R. Chen, T. Hu, W. Zhang, C. He and Y. Li, *Microporous Mesoporous Mater.*, 2021, **312**, 110739.

17 S. Xiong, X. Tang, C. Pan, L. Li, J. Tang and G. Yu, *ACS Appl. Mater. Interfaces*, 2019, **11**, 27335−27342.

18 T. Geng, S. Ye, Z. Zhu and W. Zhang, *J Mater. Chem. A*, 2018, **6**, 2808−2816.

19 Z. J. Yin, S. Q. Xu, T. G. Zhan, Q. Y. Qi, Z. Q. Wu and X. Zhao, *Chem. Commun.*, 2017, **53**, 7266−7269.

20 H. Zuo, W. Lyu, W. Zhang, Y. Li and Y. Liao, *Macromol. Rapid Commun.*, 2020, **41**, 2000489.

21 C. Wang, Y. Wang, R. L. Ge, X. D. Song, X. Q. Xing, Q. K. Jiang, H. Lu, C. Hao, X. W. Guo, Y. A. Gao and D. L. Jiang, *Chem.-Eur. J.*, 2018, **24**, 585−589.

22 X. Guo, Y. Li, M. Zhang, K. Cao, Y. Tian, Y. Qi, S. Li, K. Li, X. Yu and L. Ma, *Angew. Chem., Int. Ed.*, 2020, **59**, 22697−22705.

23 Y. Xu, H. Yu, B. Shi, S. Gao, L. Zhang, X. Li, X. Liao and K. Huang, *ACS Appl. Polym. Mater.*, 2020, **2**, 3704−3713.

24 Y. Zhao, X. Liu, Y. Li, M. Xia, T. Xia, H. Sun, Z. Sui, X.-M. Hu and Q. Chen, *Microporous Mesoporous Mater.*, 2021, **319**, 111046.

25 T. Geng, Z. Zhu, W. Zhang and Y. Wang, *J. Mater. Chem. A*, 2017, **5**, 7612−7617.

26 S. Wang, Y. Liu, Y. Ye, X. Meng, J. Du, X. Song and Z. Liang, *Polym. Chem.*, 2019, 10, 2608−2615.

27 S. An, X. Zhu, Y. He, L. Yang, H. Wang, S. Jin, J. Hu and H. Liu, *Ind. Eng. Chem. Res.*, 2019, **58**, 10495−10502.

28 Y. Wang, J. Tao, S. Xiong, P. Lu, J. Tang, J. He, M. U. Javaid, C. Pan and G. Yu, *Chem. Eng. J.*, 2020, **380**. 1222420.

29 L. Zhang, Y. Jin, G. H. Tao, Y. Gong, Y. Hu, L. He and W. Zhang, *Angew. Chem., Int. Ed.*, 2020, **59**, 20846−20851

30 X. Qian, B. Wang, Z. Q. Zhu, H. X. Sun, F. Ren, P. Mu, C. Ma, W. D. Liang and A. Li, *J. Hazard. Mater.*, 2017, **338**, 224−232.

31 H. Sun, P. La, Z. Zhu, W. Liang, B. Yang and A. Li, *J. Mater. Sci.*, 2015, **50**, 7326−7332.

32 Y. Liao, J. Weber, B. M. Mills, Z. Ren and C. F. J. Faul, *Macromolecules*, 2016, **49**, 6322−6333.

33 X. Pan, C. Ding, Z. Zhang, H. Ke and G. Cheng, *Microporous Mesoporous Mater.*, 2020, **300**, 110161.

34 M. A. Sabri, M. H. Al-Sayah, S. Sen, T. H. Ibrahim and O. M. El-Kadri, *Sci. Rep.*, 2020, **10**, 15943.

35 H. Li, X. Ding and B. H. Han, *Chem. Eur. J.*, 2016, **22**, 11863−11868.

36 X. Pan, X. Qin, Q. Zhang, Y. Ge, H. Ke and G. Cheng, *Microporous Mesoporous Mater.*, 2020, **296**. 109990.

37 Z. Yan, Y. Yuan, Y. Tian, D. Zhang and G. Zhu, *Angew. Chem., Int. Ed.*, 2015, **54**, 12733−12737.

38 Y. Sun, S. Song, D. Xiao, L. Gan and Y. Wang, *Acs Omega*, 2020, **5**, 24262−24271.

39 B. J. Riley, J. Chun, J. V. Ryan, J. Matyáš, X. S. Li, D. W. Matson, S. K. Sundaram, D. M. Strachan and J. D. Vienna, *RSC Adv.*, 2011, **1**, 1704−1715.

40 Q.-Q. Dang, X.-M. Wang, Y.-F. Zhan and X.-M. Zhang, *Polym. Chem.*, 2016, **7**, 643−647.

41 K. Xiao, H. Liu, Y. Li, G. Yang, Y. Wang and H. Yao, *Chem. Eng. J.*, 2020, **382**, 122997.

42 M. Rong, L. Yang, L. Wang, H. Xing, J. Yu, H. Qu and H. Liu, *Ind. Eng. Chem. Res.*, 2019, **58**, 17369.

43 Y. Chen, H. Sun, R. Yang, T. Wang, C. Pei, Z. Xiang, Z. Zhu, W. Liang, A. Li and W. Deng, *J. Mater. Chem. A*, 2015, **3**, 87−91.

44 A. Sigen, Y. Zhang, Z. Li, H. Xia, M. Xue, X. Liu and Y. Mu, *Chem. Commun.*, 2014, **50**, 8495−8498.
45 C. Pei, T. Ben, S. Xu and S. Qiu, *J. Mater. Chem. A*, 2014, **2**, 7179−7187.
46 D. F. Sava, K. W. Chapman, M. A. Rodriguez, J. A. Greathouse, P. S. Crozier, H. Zhao, P. J. Chupas and T. M. Nenoff, *Chem. Mater.*, 2013, **25**, 2591−2596.
47 X. Zhang, I. Silva, H. G. W. Godfrey, S. K. Callear, S. A. Sapchenko, Y. Cheng, I. Vito´rica-Yreza´bal, M. D. Frogley, G. Cinque, C. C. Tang, C. Giacobbe, C. Dejoie, S. Rudic´, A. J. Ramirez-Cuesta, M. A. Denecke, S. Yang and M. Schro¨der, *J. Am. Chem. Soc.*, 2017, 139, 16289−16296.
48 L. Lin, H. Guan, D. Zou, Z. Dong, Z. Liu, F. Xu, Z. Xie and Y. Li, *RSC Adv.*, 2017, **7**, 54407−54415.
49 D. F. Sava, M. A. Rodriguez, K. W. Chapman, P. J. Chupas, J. A. Greathouse, P. S. Crozier and T. M. Nenoff, *J. Am. Chem. Soc.*, 2011, 133, 12398−12401.
50 K. W. Chapman, P. J. Chupas and T. M. Nenoff, *J. Am. Chem. Soc.*, 2010, **132**, 8897−8899.